Critical magnetic properties of disordered polycrystalline $Cr_{75}Fe_{25}$ and $Cr_{70}Fe_{30}$ alloys

S. F. Fischer,[1,*] S. N. Kaul,[1,2] and H. Kronmüller[1]
[1]*Max-Planck-Institut für Metallforschung, Postfach 80 06 65, 70569 Stuttgart, Germany*
[2]*School of Physics, University of Hyderabad, Central University P.O., Hyderabad - 500046, Andhra Pradesh, India*
(Received 14 September 2000; revised manuscript received 10 October 2001; published 24 January 2002)

Critical magnetic properties of disordered polycrystalline $Cr_{75}Fe_{25}$ and $Cr_{70}Fe_{30}$ alloys are investigated employing bulk magnetization and, for the first time to our knowledge, low-field ac susceptibility measurements. Contrary to the earlier claims, an elaborate analysis of high-precision magnetization and ac susceptibility data reveals that long-range ferromagnetic order exists, and that a true ferromagnetic to paramagnetic phase transition takes place in the chemically homogenized alloys. Chemical clustering leads to superparamagnetic behavior above and inhomogenous magnetization below the Curie temperature, complicating the experimental determination of the asymptotic critical exponents, particularly when high-field extrapolation methods are used. The effective critical exponents possess the values $\beta_{\text{eff}}=0.30\pm0.01$, $\gamma_{\text{eff}}=1.39\pm0.01$, and $\delta_{\text{eff}}=5.5\pm0.1$ for chemically homogenized samples. These values deviate substantially from the estimates based on three- or two-dimensional isotropic ''short-range'' models. The presently determined values for the critical exponents instead indicate that the critical behavior of $Cr_{75}Fe_{25}$ and $Cr_{70}Fe_{30}$ is akin to that of a $d=2,n=1$ ferromagnet in which the attractive long-range interactions between spins decay with distance (r) as $J(r)\sim r^{-(d+\sigma)}$ with $\sigma=1.4$.

DOI: 10.1103/PhysRevB.65.064443 PACS number(s): 75.40.Cx, 05.70.Jk, 75.50.Bb

I. INTRODUCTION

Magnetic properties of Cr-Fe alloys have fascinated experimentalists[1–21] as well as theorists[22–27] for decades, since complex magnetic phenomena are conveniently studied in such alloys throughout the *whole* composition range of the chemical phase diagram. bcc-Fe behaves as a typical (itinerant) ferromagnet below a Curie temperature of $T_C=1044$ K, while bcc-Cr, an (itinerant) antiferromagnet, exhibits complicated spin structures such as longitudinal and transverse spin-density waves below a Néel temperature of $T_N=312$ K. The most frequently cited magnetic phase diagram of Fe-Cr was compiled and discussed by Burke and co-workers.[10–12] The collinear ferromagnetism of Fe progressively paves the way to a more and more inhomogeneous magnetic order with increasing Cr content, resulting in monotonically reduced values of the Curie temperature. A ''crossover'' regime of chemical composition ranging between 20- and 30-at. % Fe is characterized by low Curie temperatures (lower than 300 K) and a re-entrant spin glasslike behavior at low temperatures. At lower Fe content, two critical concentrations exist: below 19-at. % but above 16-at. % Fe, a spin-glass-like phase is found,[11] and below 16-at. % Fe antiferromagnetism is observed.[10] Nevertheless, many issues remain to be resolved. In particular, a complete understanding of magnetism in the crossover regime from ferromagnetism to a spin-glass-like state is lacking at present. Specifically, the following questions need answers. Does long-range ferromagnetism persist down to 20-at. % Fe? If so, what is the nature of the ferromagnetic (FM) to paramagnetic (PM) phase transition? How does chemical short-range clustering affect magnetism for Fe concentrations between 20 and 30 at. %?

Several authors[5–8,11,12,16,20] claimed that long-range ferromagnetic order exists in the alloys with the Fe concentration around 25 at. %. Inhomogeneous magnetization is often taken to manifest itself in unusually large values of the effective critical susceptibility exponent γ_{eff}. Values of γ_{eff} as large as 2.0 were reported by Aldred and Kouvel[8] (to our knowledge the only investigation on critical magnetic properties of $Cr_{75}Fe_{25}$ and $Cr_{70}Fe_{30}$ alloys). Other authors[17–19] questioned the existence of long-range ferromagnetic ordering and a well-defined FM-PM phase transition in these alloys, and attributed the magnetic properties of these alloys to superparamagnetic clusters (also referred to as ''giant moments'' or ''mictomagnetic'' particles).

Conflicting reports, based on bulk magnetization,[3–5,7,8] neutron-scattering,[6,11,12,16] and Mössbauer[1,2,9,13–16,18] data, about the nature of ferromagnetic-paramagnetic phase transition in Cr-rich Fe alloys, with an Fe concentration near the critical concentration of ferromagnetism and enhanced experimental resolution that recent advances in technology permit, prompted us to perform extensive high-precision bulk magnetization and ac susceptibility measurements of well-characterized polycrystalline samples of two alloys in the crossover composition range, i.e., on $Cr_{75}Fe_{25}$ and $Cr_{70}Fe_{30}$ alloys. Magnetic measurements were carried out on as-cast and homogenized specimens, with a view to investigate the influence of chemical short-range order on magnetic properties. The main concern of the present experiments is to conclusively support or refute the existence of long-range ferromagnetic order and a well-defined FM-PM phase transition in the alloys in question.

II. EXPERIMENTAL DETAILS

Alloys with nominal compositions of $Cr_{75}Fe_{25}$ and $Cr_{70}Fe_{30}$ were prepared by rf-induction melting under an inert high-purity argon atmosphere. The purity of the starting elements was as follows: for $Cr_{75}Fe_{25}$, 99.99-at. % Cr and 99.98-at. % Fe (which compares well with that of other

works); for $Cr_{70}Fe_{30}$, 99.998-at. % Cr and 99.999-at. % Fe.

In order to ensure good chemical homogeneity, the ingots were remolten several times. Detailed chemical and microstructural analyses were carried out by x-ray fluorescence spectroscopy, wavelength- and energy-dispersive x-ray scattering (WDS, EDS) and Bragg x-ray-diffraction measurements. Spherical samples (of ~2.6-mm diameter) were spark machined to insure a well-defined macroscopic geometry for considerations of demagnetization effects. Subsequently, the specimen surface was etched and cleaned by repeated rinsing in ethanol and distilled water. Samples that underwent a homogenizing anneal were sealed in quartz tubes in a high-purity argon atmosphere with a suitable pressure for long-term high-temperature heat treatment. Annealing, carried out at 1323 K for 7–21 days, was followed by a water quench. Initially, the annealing parameters were chosen to be the same as those used in Ref. 10, and subsequently, the annealing time was adjusted after observing changes in magnetic properties (i.e., a sharpening of the kink point). Electron-beam heating in vacuum, which allows annealing in a high-purity environment, was attempted as well, but had to be discarded as slow cooling rates work against the homogenizing process.

ac susceptibility (χ_{ac}) measurements were performed on a Lakeshore model 7229 susceptometer in an ac-driving field of amplitude $\mu_0 H_{ac} = 0.1$ mT and a frequency of 110 Hz (using the extraction method). For investigating critical phenomena, χ_{ac} data were taken at 0.2 K intervals in the temperature range $\epsilon = (T - T_C)/T_C \leqslant 0.15$. Care was taken to demagnetize the measurement environment at 300 K before taking the data to prevent remanent rest fields, which invariably led to erroneous results for the zero-field susceptibility χ_0.

Magnetization versus external field (H_{ext}) isotherms were measured using a SQUID magnetometer (QMPMS-2) at intervals ranging from 0.5 to 0.05 K (at a temperature stability better than ± 30 mK) in fields up to 2 T. The raw data were corrected for the temperature shift, the demagnetization of the sample, and the remanent effects inherent to the measurement technique. For this purpose, the demagnetization factor was determined from dc susceptibility in low fields $\leqslant 2$ mT.

III. EXPERIMENTAL RESULTS

A. Chemical analysis

X-ray fluorescence (XRF) analysis revealed a chemical composition (within experimental error) close to the nominal value for each alloy; for $Cr_{75}Fe_{25}$, 74.64 ± 0.5-at. % Cr and 25.0 ± 0.14-at. % Fe, for $Cr_{70}Fe_{30}$, 70.6 ± 0.5-at. % Cr and 29.4 ± 0.2-at. % Fe. Therefore, these alloy specimens are henceforth referred to as $Cr_{75}Fe_{25}$ and $Cr_{70}Fe_{30}$.

To gain insight into the spatial distribution of chemical composition and the microstructure, fine-polished samples (from those regions of ingot that were used for making the spherical specimens) were examined by EDS and WDS. A typical EDS (back scattering) micrograph, shown in Fig. 1, indicates grains (of average diameter 20–50 μm), holes (dark), and small (light) particles of a few μm mostly at the grain boundaries. WDS measurements (experimental resolution better than 0.5 at. %) confirm that the chemical composition of grains is near the nominal compositions whereas the small particles are nothing but Cr-rich regions with a Cr-content up to 99.5 at. %. Therefore, not all of the Cr dissolves in the melt, and the Cr content of grains is expected to be slightly lower than measured by XRF. Nevertheless, Cr-rich particles are estimated to occupy 0.03 % of the total sample volume and are, therefore, of no consequence so far as the investigation of the existence (or otherwise) of long-range ferromagnetic order is concerned. Detailed WDS examination rules out a spatial gradient of the chemical composition of more than 0.5 at. % on a length scale of 1 μm within grains or across grain boundaries. Annealing at 1323 K for seven days followed by a water quench causes an increase in the average value of the Cr content in grains by 0.6–0.7 at. %. Hence we conclude that Cr of the Cr-rich regions (μm-small particles) dissolves by annealing into the Cr-Fe alloy matrix of the grains.

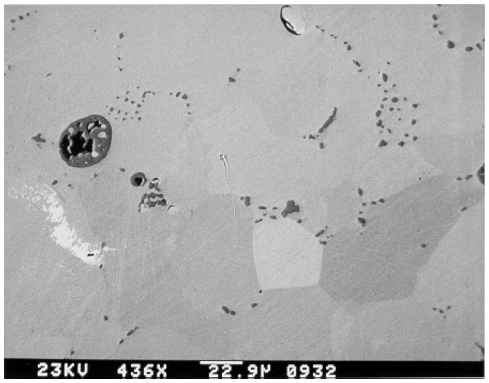

FIG. 1. $Cr_{75}Fe_{25}$: typical EDS micrograph of the grain structure in polished as-cast specimen. The average grain diameter ranges from 60 to 100 μm. Dark spots of 1 μm in size represent Cr-rich particles, while black spots depict holes.

X-ray-diffraction patterns revealed only the fundamental bcc crystal structure but no reflections of the superstructure peaks. Thus the CrFe alloys are in a disordered state.

B. Low-field dc and ac susceptibility

1. Temperature dependence

According to the ''kink-point'' method,[28] the Curie temperature T_C of ferromagnets can be estimated from low-field susceptibility measurements by the kink-point temperature T_k which characterizes the first departure (decrease) from the demagnetization-limited value of susceptibility $\chi(T)$. Annealing and subsequent quenching of Cr-rich Fe-Cr alloys lowers T_k drastically, as illustrated by the data presented in Fig. 2. The low-field (10 mT) dc susceptibility of the as-cast specimen [Fig. 2(a)] decreases with increasing temperature over a broad temperature range (150 to >300 K) and T_k (at about 180 K) is not well defined. After a heat treatment at 1323 K for seven days and a water quench [Fig. 2(b)], T_k is lowered to about 140 K and the kink point has sharpened. For a prolonged annealing time [Fig. 2(c)], the temperature

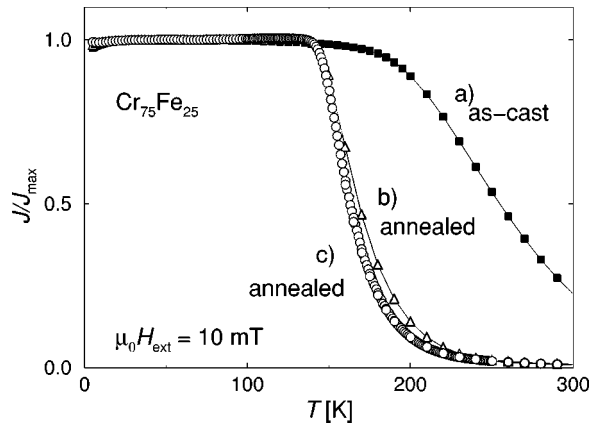

FIG. 2. $Cr_{75}Fe_{25}$: annealing effects on the temperature dependence of low-field (10 mT) dc susceptibility. After annealing treatment the kink-point temperature T_k of the sample decreases drastically. (a) As-cast specimen, (b) After seven days at 1323 K and quenched by water. (c) Seven plus 14 days at 1323 K, and quenched by water.

range above T_k over which $\chi(T)$ decreases narrows further, and the change in $\chi(T)$ at 300 K is negligible.

From the temperature dependence of the ac susceptibility $\chi(T)$ at an applied field of 0.1 mT, the (effective) demagnetization factors of the samples were extracted by plotting the inverse low-field susceptibility which corresponds for low fields and $T<T_C$ to $1/(4\pi\chi)\simeq N$. The inset of Fig. 3 demonstrates this for the spherical $Cr_{75}Fe_{25}$ sample, (a) as cast and (b) after a homogenizing heat treatment.

$\chi(T)$ of the as-cast specimen is demagnetization limited only up to $T\sim 100$ K, with an effective demagnetization factor of $N\simeq 0.36$. After annealing $\chi(T)$ is demagnetization limited from 120 K$<T<$140 K, yielding a lowered effective demagnetization factor of $N\simeq 0.35$. As the macroscopic geometry of the sample remains unchanged, it follows that annealing (with subsequent water quench) leads to a spatially homogenized magnetization distribution because the theoretical value of 0.33 for a homogenously magnetized sphere is approached.

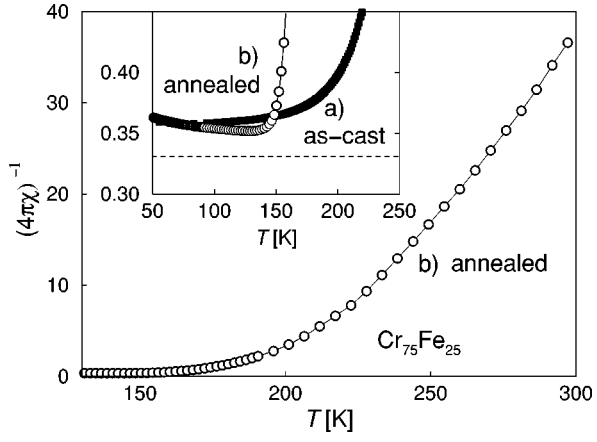

FIG. 3. $Cr_{75}Fe_{25}$: temperature dependence for the inverse ac susceptibility $1/\chi(T)$ ($\mu_0 H_{ac}=0.1$ mT, $H_{dc}=0$, $\nu=110$ Hz). The inset (same measure quantities) shows an enlargement of the demagnetization-limited values for temperatures up to T_k for (a) the as-cast specimen and (b) the specimen after annealing treatment.

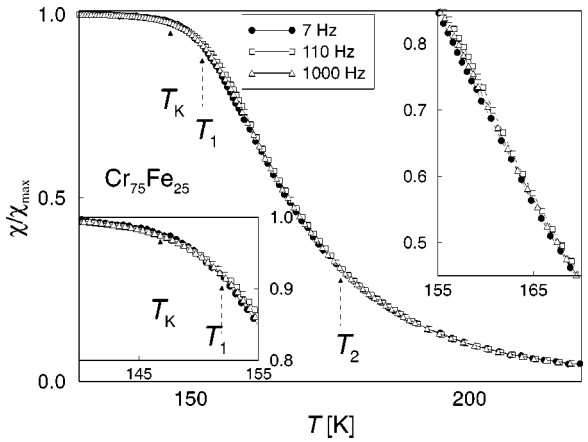

FIG. 4. $Cr_{75}Fe_{25}$: the frequency dependence of the ac susceptibiliy for temperatures around the kink-point temperature T_k ($\mu_0 H_{ac}=0.1$ mT, $H_{dc}=0$, and $\nu=7$, 110, and 1000 Hz). The left inset enlarges the temperature region of T_k. The right inset highlights the frequency dependence of $\chi(T)$ in the temperature interval $T_1\leqslant T\leqslant T_2$. The insets measure quantities given by the graph axes.

Above T_k a convex curvature of $\chi^{-1}(T)$ up to 300 K is found for all samples, and demonstrates that no simple Curie-Weiss behavior exists, signaling the existence of superparamagnetic clusters. The paramagnetic moment per alloy atom is given by $\mu_{\rm eff}^p = p_{\rm eff}\mu_B$, where $p_{\rm eff}=g\sqrt{S(S+1)}=\sqrt{q_c(q_c+2)}$, $S=(1/2)q_c$ is the effective spin per atom, q_c the number of magnetic carriers per atom, and the Landé factor is $g\simeq 2$ (transition metals). Experimentally, $p_{\rm eff}$ is determined by

$$p_{\rm eff}(T)=\left(\frac{3k_B}{N}\right)^{1/2}\left(\frac{d(\chi^{-1})}{dT}\right)^{-1/2}\frac{1}{\mu_B}, \qquad (1)$$

where N is the number of atoms, k_B is the Boltzmann constant and μ_B is the Bohr magneton. $p_{\rm eff}$ attains a constant value at high temperatures where the temperature derivative of χ^{-1} is temperature independent.

2. Frequency dependence

The frequency dependence of the low-field ac susceptibility kink point was checked by applying an ac-driving field of rms amplitude 0.1 mT and frequencies of 7, 110, and 1000 Hz.

As expected for a true FM-PM thermodynamic phase transition, no systematic shift of the kink-point temperature T_k with frequency is observable in Fig. 4; a shift of 0.1% of T_k would have been easily discernible. However, small deviations of 0.14% of T_k (=0.2 K) are detected (Fig. 4) *above* T_k, in a range between $T_1=152$ K and $T_2=180$ K, which is the region of strongest decrease in $\chi(T)$. Such deviations are indicative of the presence of finite magnetic clusters of asorted sizes. Above T_2 the $\chi(T)$ curves taken at different frequencies once again match. The absence of a frequency dependence above T_2 shows that (a) a narrowing of the size distribution of finite magnetic clusters for temperatures above T_2, occurs, so much so that the frequency dependence

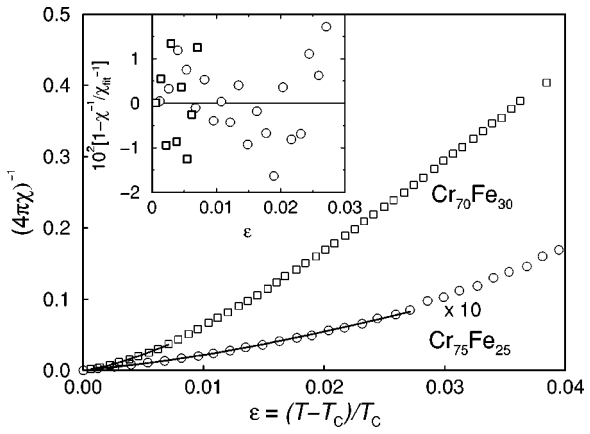

FIG. 5. $Cr_{75}Fe_{25}$ (T_C=145.05 K) and $Cr_{70}Fe_{30}$ (T_C=256.02 K): the inverse ac susceptibility data $\chi^{-1}(T)$ ($\mu_0 H_{ac}$=0.1 mT, H_{dc}=0, and ν=110 Hz) are depicted by the open circle ($Cr_{75}Fe_{25}$) and square ($Cr_{70}Fe_{30}$) symbols. The lines represent the power-law fits to the $\chi^{-1}(T)$ within the ACR, based on Eq. (2) with γ_{eff}=1.39. The inset displays the percentage deviation of the $\chi^{-1}(T)$ data from the power law fits in the ACR.

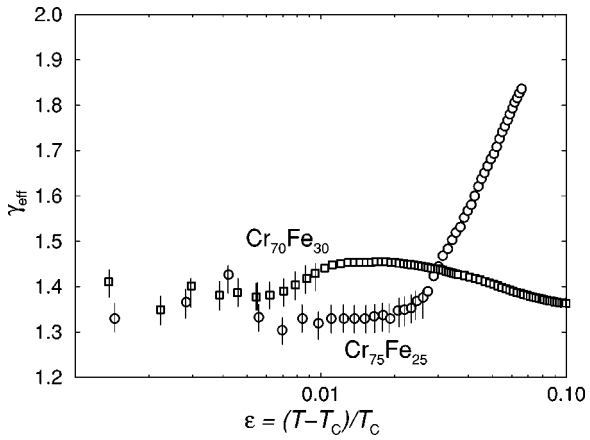

FIG. 6. $Cr_{75}Fe_{25}$ and $Cr_{70}Fe_{30}$: temperature dependence of γ_{eff}. The vertical lines depict uncertainties given by the ''range-of-fit'' analysis in the asymptotic critical temperature regime.

of $\chi(T>T_2)$ is below the observation limit; and (b) the overall magnetic cluster size above T_2 reduces to such an extent that their relaxation times are less than 1 msec.

3. Analysis of critical properties

The foregoing results give confidence that the chemically homogenized samples can be investigated in terms of critical phenomena. ac susceptibility measurements provide the most direct means of determining the zero-field susceptibility χ_0, and hence T_C and the critical exponent γ. Difficulties arising from high-field extrapolation procedures are avoided as the true initial susceptibility is directly obtained if stray fields of the measurement environment are avoided.

An elaborate ''range-of-fit'' (ROF, described in detail elsewhere[29]) analysis, based on the power law, of the susceptibility data corrected for demagnetizing effects, yields the asymptotic critical range of the FM-PM phase transition, the transition temperature and the critical exponent γ, defined as

$$\chi_0(T) \sim \epsilon^{-\gamma}, \tag{2}$$

where the reduced temperature $\epsilon=(T-T_C)/T_C$. The ROF analysis for $Cr_{75}Fe_{25}$ yields the least-squares fit (Fig. 5) over the largest temperature range for the choice γ_{eff}=1.36(3) and T_C=145.0(1) K.

Within the asymptotic critical regime (ACR) of $1.2\times10^{-3}\leq\epsilon\leq2\times10^{-2}$, γ_{eff} is constant within the error limits (Fig. 6). For $\epsilon>0.02$, γ_{eff}(T) shows a monotonic increase which is understood by remaining short-range chemical order that gives rise to magnetically ordered finite regions.[29] For $Cr_{70}Fe_{30}$, the analysis gives γ_{eff}=1.39(1) and T_C=256.0(1) K with an ACR of $6.4\times10^{-4}\leq\epsilon\leq1\times10^{-2}$. For $\epsilon>0.01$, γ_{eff}(T) increases, shows a maximum of 1.45 at $\epsilon\sim0.02$, and decreases below 1.39 for larger ϵ. Such a behavior is well known[29] for disordered amorphous alloys, and it follows that the degree of magnetic inhomogenity for $Cr_{70}Fe_{30}$ is reduced compared to that of $Cr_{75}Fe_{25}$. The *temperature-independent* value (Fig. 6) of γ_{eff}, within the uncertainty limits, for both alloys indicates that $\gamma_{eff}\simeq\gamma$ (*asymptotic* critical exponent) and the ''correction-to-scaling'' terms are negligibly small. This conclusion is further supported by the finding that the above parameter values (Table I) remain practically *unaltered* when the theoretical fits to the susceptibility data (in the ACR) take into account the leading correction-to-scaling term, i.e., when the expression $\chi_0(T)=A\epsilon^{-\gamma}(1+B\epsilon^{\Delta})$ with[29] Δ=0.55 is used instead of Eq.(2), and the quality of the fits does not improve.

C. Bulk magnetization

Isotherms of magnetization from high fields of 9 or 7 T down to 0 T show little, or even no, effect of annealing at

TABLE I. Results of bulk magnetization (BM) and ac susceptibility (ACS) data analyses. Magnetic parameters of interest are given in cgs units to facilitate comparison with previous works (Refs. 8 and 29). The number in parentheses represents the uncertainty of in the least significant figure.

	$Cr_{75}Fe_{25}$	$Cr_{70}Fe_{30}$
T_C (K)	145.0(1)	256.0(1)
σ_0 (emu/G)	43.2	56.7
μ_0 (μ_B/at. %)	0.41(1)	0.54
m_0 (emu/g)	37.4(5)	42.7(2)
h_0 (KOe)	74.8(5)	119(15)
m_0/σ_0	0.9(1)	0.75(3)
$\frac{\mu_0 h_0}{k_B T_C}$	0.0142	0.017
$\mu^*(\mu_B)$	46	51
$c^*=\mu_0/\mu^*$ (%)	0.9	1.05
ACS: γ_{eff}	1.36(3)	1.39(3)
[Fit range ($10^3\epsilon$)]	[1.2-20]	[0.64-10]
BM: γ_{eff}	1.39(1)	1.39(1)
[Fit range ($10^3\epsilon$)]	[1.6-40]	[0.96-31]
BM: β_{eff}	0.30(1)	0.315(5)
[Fit range ($10^3\epsilon$)]	[0.16-29]	[0.56-20]
BM: δ_{eff}	5.5(1)	5.36(4)
$\delta_{eff}^{calc}=1+\gamma/\beta$	5.6(2)	5.4(1)

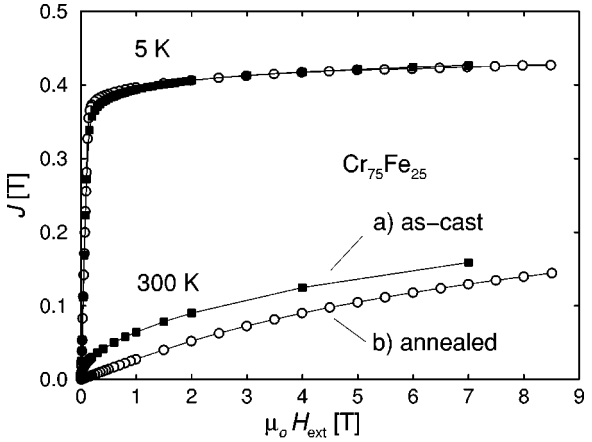

FIG. 7. $Cr_{75}Fe_{25}$: magnetic isotherms (a) of the as-cast specimen (closed square symbols) and (b) after annealing (open circle symbols), at 5 and 300 K.

low temperatures. The saturation moment per alloy atom at 5 K for $Cr_{75}Fe_{25}$ remains the same before and after annealing, as shown in Fig. 7, but this is not the case at 300 K: a decrease in the field-induced moment and curvature of the isotherm, consequent upon annealing and subsequent water quench, is evident in Fig. 7. The field response at 300 K before and after annealing is nonlinear, as against the linear one expected in the paramagnetic region for localized moments. The nonlinear field dependence is well described by the field response of superparamagnetic clusters, which for the as-cast sample are larger in size than after annealing. In the following, isotherms taken in the vicinity of the kink-point temperature are evaluated in terms of different forms of scaling equations of state, that are generally used to extract accurate values of T_C and the critical exponents β and γ.

1. Arrott plots

For any spin system with a long-ranged ferromagnetic interaction exhibiting a mean-field critical behavior (γ=1.0, β=0.5), Arrott plot[30] isotherms are nothing but a set of straight and parallel isotherms in the immediate vicinity of the Curie temperature. In disordered ferromagnets too, where higher-order terms[29] in the expansion of field in powers of magnetization become important, Arrott plots are useful in determining the critical exponents. In such a case, a quadratic extrapolation yields reliable results. Considering the possible presence of long-range interactions as well as disorder in Cr-rich Fe-Cr alloys, such an evaluation appears meaningful.

The Arrott plot constructed out of the isotherms taken on $Cr_{75}Fe_{25}$ is shown in Fig. 8 for fields ranging between 0.02 and 2 T. The anomalously large critical exponents, reported previously by Aldred and Kouvel,[8] were obtained from Arrott plots in the field range 0.025 to 1.5 T. A strong curvature persists over the entire field range. The curves are parallel down to fields of about 1 T. For small fields, the distance between different isotherms continuously decreases. Such a strong curvature of the isotherms renders the intercepts on axes obtained by extrapolation unreliable. Even quadratic extrapolation does not reproduce the data over a large field

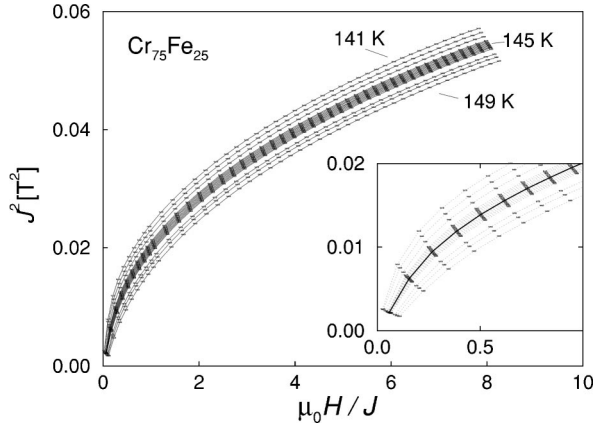

FIG. 8. $Cr_{75}Fe_{25}$ (heat treated and water quenched): Arrott plots of the isotherms taken from 141 to 149 K. Large spacings are 1-K intervals, small spacings at 0.2-K intervals. The inset highlights the low-field region (with same measure quantites as in the graph). The critical isotherm corresponds to a temperature close to 145 K (solid line).

range and as such the extrapolated zero-field values cannot be relied upon. Due to the large uncertainty of the results from such extrapolation, we do not follow this procedure further. Nevertheless, the Arrott plot indicates that the critical isotherm, which passes through the origin, for $Cr_{75}Fe_{25}$ is in the vicinity of 145 K (the dark solid line in Fig. 8).

2. Modified Arrott plot (MAP) analysis

The scaling equation of state, proposed by Arrott and Noakes,[31] forms the basis of a common method to determine the critical exponents β and γ from magnetization data taken in finite fields, and is given by

$$(\mu_0 H/J)^{1/\gamma} = a\epsilon + bJ^{1/\beta}, \tag{3}$$

where a and b are coefficients. In the so-called modified Arrott plot (MAP) method, the $J(H,T)$ isotherms plotted in the form $J^{1/\beta}$ against $(\mu_0 H/J)^{1/\gamma}$ give a set of parallel straight lines for temperatures in the immediate vicinity of T_C for specific choices of the exponents β and γ. The critical

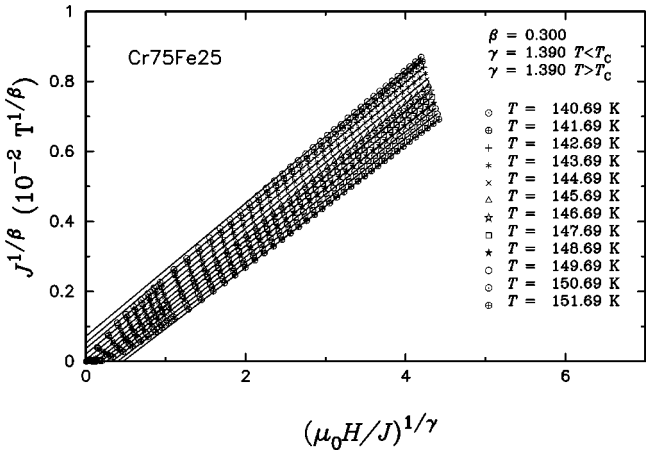

FIG. 9. $Cr_{75}Fe_{25}$: modified Arrott plot. For the sake of clarity only isotherms in temperature intervals of 1 K are plotted.

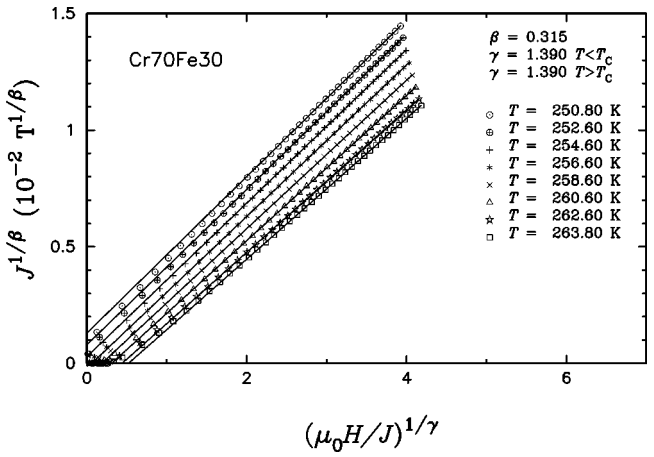

FIG. 10. $Cr_{70}Fe_{30}$: modified Arrott plot. For the sake of clarity only isotherms in temperature intervals of about 2 K are plotted.

isotherm ($T=T_C$) passes through the origin. Ideally, the spontaneous magnetization $J_s(T)$ and the inverse initial zero-field susceptibility $\chi_o^{-1}(T)$ are computed from the intercepts of the straight-line isotherms on the ordinate ($T<T_C$) and abscissa ($T>T_C$) of the MAP. In practice, for many systems, extrapolation from high-field values is necessary because for low fields the isotherms deviate from the straight-line behavior. The values for the exponents β and γ, as well as T_C, are subsequently refined by employing the Kouvel-Fisher (KF) analytical method,[32] which is based on the expressions

$$J_s\left(\frac{dJ_s}{dT}\right)^{-1}=\frac{(T-T_C)}{\beta} \tag{4}$$

and

$$\chi_o^{-1}\left(\frac{d\chi_o^{-1}}{dT}\right)^{-1}=\frac{(T-T_C)}{\gamma}, \tag{5}$$

valid in the asymptotic critical region. The quantities $Y(T)\equiv J_s(dJ_s/dT)^{-1}$ and $X(T)\equiv\chi_o^{-1}(d\chi_o^{-1}/dT)^{-1}$ are calculated from a cubic spline which was fitted to $J_s(T)$ and $\chi_o^{-1}(T)$ (Fig. 11 and 13). Plots of $Y(T)$ and $X(T)$ against T yield straight lines with slopes of $1/\beta$ and $1/\gamma$, respectively, on which the intercept on the T axis is equal to T_C. To arrive at the most accurate values of β, γ, and T_C, the values resulting from the KF method are used to reconstruct the MAP. This iteration process is followed until two successive runs leave $J_s(T)$ and $\chi_o^{-1}(T)$, and hence β and γ, unaltered. This method is referred to elsewhere[29] as a *modified asymptotic analysis*. Figures 9 –14 show the outcome of the iterative MAP-KF analysis on isotherms of the homogenized $Cr_{75}Fe_{25}$ and $Cr_{70}Fe_{30}$ spheres.

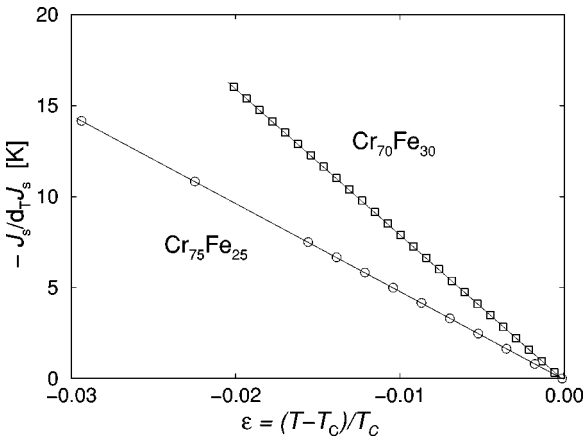

FIG. 12. $Cr_{75}Fe_{25}$ and $Cr_{70}Fe_{30}$: Kouvel-Fisher plot to determine β and T_C.

The observations of MAP-analysis modified for $Cr_{75}Fe_{25}$ are as follows.

(i) A straightening of isotherms is best for $\beta_{\text{eff}}=0.30(1)$, and $\gamma_{\text{eff}}=1.39(1)$ giving a value of $T_C=144.9(1)$ K.

(ii) This set of values is stable (within error limits) against iterative usage of Kouvel-Fisher extrapolation and the MAP.

(iii) Any effort to increase β_{eff} leads to an increased concave downward curvature.

(iv) As discussed elsewhere,[29] the nonlinearity in MAP isotherms is more pronounced below T_C than above.

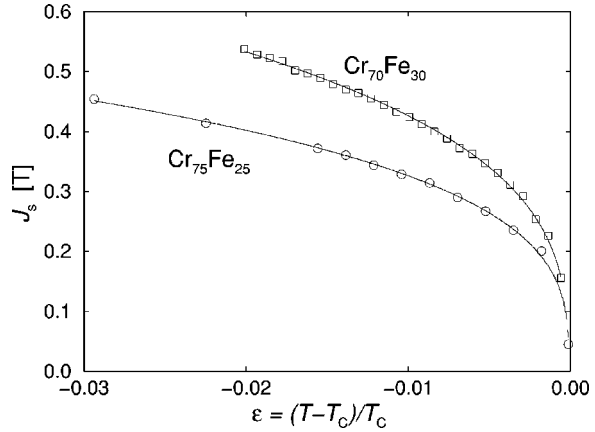

FIG. 11. $Cr_{75}Fe_{25}$ and $Cr_{70}Fe_{30}$: temperature dependence of the spontaneous magnetization $J_S(T)$ resulting from high-field extrapolation of the modified Arrott plots shown in Figs. 9 and 10.

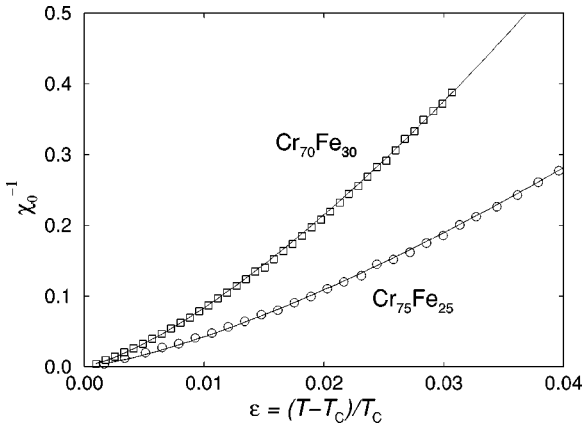

FIG. 13. $Cr_{75}Fe_{25}$ and $Cr_{70}Fe_{30}$: temperature variation of the inverse initial susceptibility $\chi_o^{-1}(T)$ resulting from a high-field extrapolation of the modified Arrott plots shown in Figs. 9 and 10.

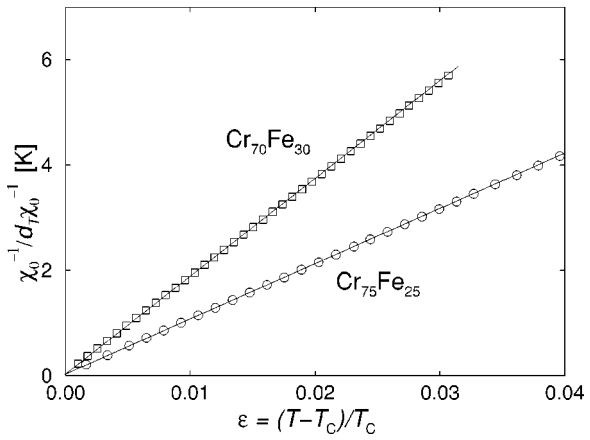

FIG. 14. $Cr_{75}Fe_{25}$ and $Cr_{70}Fe_{30}$: Kouvel-Fisher plot to determine γ and T_C.

The field dependence of the critical isotherm is governed by the power law

$$J(T=T_C)\sim H^{1/\delta}. \tag{6}$$

$Cr_{75}Fe_{25}$ isotherms in the vicinity of T_C, when plotted in the form of $\ln J$ vs $\ln H$, yield $\delta_{\rm eff}=5.5(1)$ (shown in Fig. 15). This value compares well with that calculated using the presently determined values of $\gamma_{\rm eff}$ and $\beta_{\rm eff}$ in the scaling relation $\delta_{\rm eff}^{\rm calc}=1+\gamma_{\rm eff}/\beta_{\rm eff}=5.6(2)$.

The asymptotic analysis, described above, was likewise applied to the isotherms taken on a well-homogenized $Cr_{70}Fe_{30}$ sphere. The resulting exponents are similar to that of $Cr_{75}Fe_{25}$ (see Figs. 11, 12, 13, 14, and 16), and are given in Table I.

3. Scaling equation of state A

Magnetization data with the values of the exponents determined by MAP-KF analysis satisfy the scaling equation of state (SES) of the form

$$J|\epsilon|^{-\beta}=f_{\pm}(H|\epsilon|^{-(\gamma+\beta)})=f_{\pm}(h), \tag{7}$$

where $f_{\pm}(h)$ are scaling functions for temperatures above and below T_C, respectively, as demonstrated by the double-logarithmic plots shown in Figs. 17 and 18. However, due to the insensitive nature of the log-log scale, many sets of T_C, $\beta_{\rm eff}$, and $\gamma_{\rm eff}$ values yield nearly the same quality of data collapse.

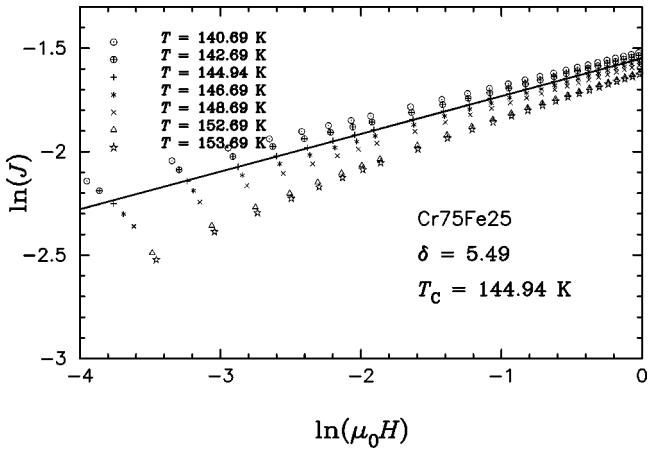

FIG. 15. $Cr_{75}Fe_{25}$: The critical isotherm in a $\ln J$ vs $\ln H$ isotherm is linear for fields $\geqslant$70 mT.

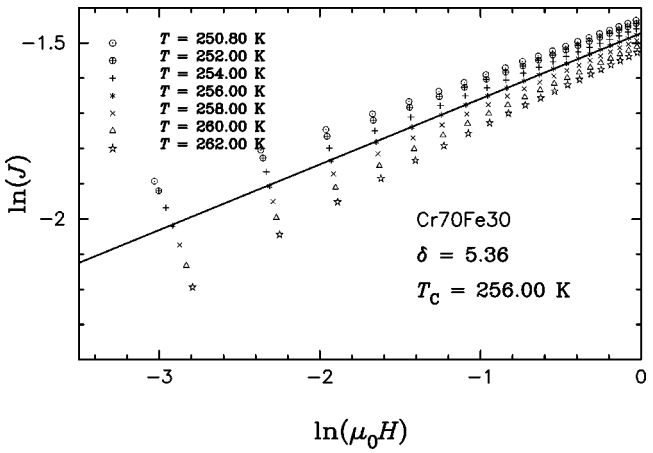

FIG. 16. $Cr_{70}Fe_{30}$: the critical isotherm in a $\ln J$ vs $\ln H$ isotherm is linear for fields $\geqslant$28 mT.

4. Scaling equation of state B

In contrast, the following scaling equation of state is sensitive to very small deviations

$$h/m=\pm a_{\pm}+b_{\pm}m^2, \tag{8}$$

where the plus and minus signs depict the temperature ranges above and below T_C, respectively; $m=M/\epsilon^{\beta}$ is the reduced magnetization, and $h/m=(H/M)\epsilon^{-\gamma}$ the reduced inverse susceptibility.

Nevertheless, other sets of values for the parameter triples T_C, $\beta_{\rm eff}$, and $\gamma_{\rm eff}$ also produce scaling plots of similar quality so that this method fails to distinguish between different sets of values as well. In particular, unusually high exponent values for $Cr_{75}Fe_{25}$ as $\beta=0.44$ and $\gamma=2.0$, similar to those reported by Aldred and Kouvel[8] ($\beta=0.47$, $\gamma=2.03$), satisfy Eq. (8) but with a different choice of T_C. This uncertainty in

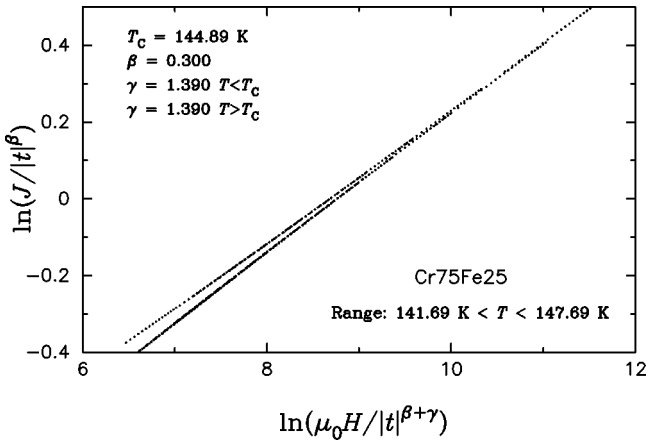

FIG. 17. $Cr_{75}Fe_{25}$: according to the scaling hypothesis, two branches for $T<T_C$ and $T>T_C$ exist for the given choices of γ, β, and T_C. Here t depicts $\epsilon=|T-T_C|/T_C$.

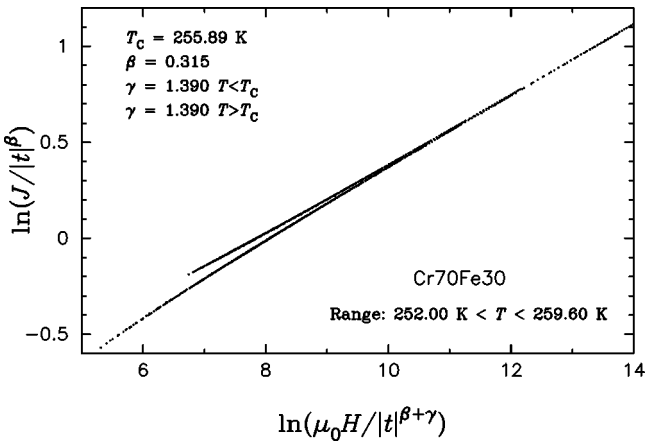

FIG. 18. $Cr_{70}Fe_{30}$: according to the scaling hypothesis two branches for $T<T_C$ and $T>T_C$ exist for the given choices of γ, β, and T_C. Here t depicts $\epsilon=|T-T_C|/T_C$.

exponent values obtained from the SES forms [Eqs. (7) and (8)] is a direct outcome of the *three free* parameters involved while only *two* parameters are free in the case of the MAP.

The intercepts on the m^2 and h/m axes (Fig. 19), m_0^2 and h_0/m_0, often considered as the *average* effective spontaneous magnetization and the *average* effective exchange field, are given in Table I. Following Aldred and Kouvel,[8] the effective elementary moment taking part in the ordering process is defined as μ^* and calculated by equating $\mu^* h_0/k_B T_C$ to the theoretical value[29] of 1.6. The value of μ^* turns out to be 46 μ_B (16μ_B in Ref. 8), and the concentration of such giant moments equals of 0.9% (2.6% in Ref. 8).

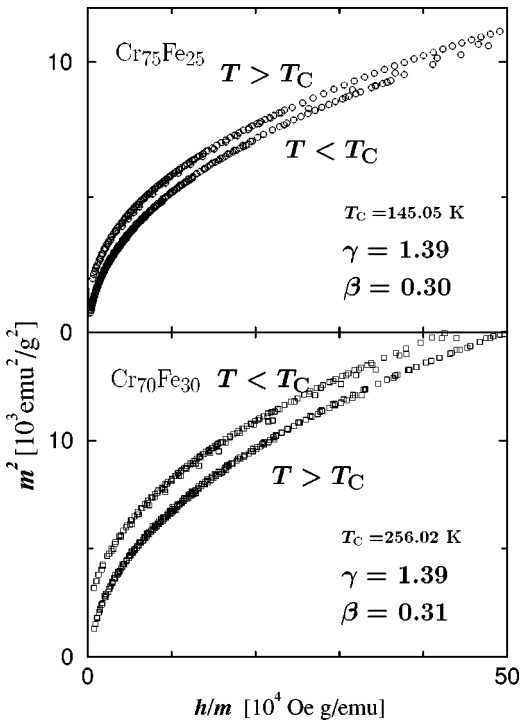

FIG. 19. $Cr_{75}Fe_{25}$ and $Cr_{70}Fe_{30}$: scaling plots according to the scaling equation of state (8). Isotherms ($\Delta T=1$ K, $H_{ext}>0.1$ T) fall on two universal curves for $T<T_C$ and $T>T_C$ for the given choices of γ, β, and T_C. Magnetization and magnetic field are given in cgs units so as to facilitate comparision with other works (Refs. 8 and 29).

IV. DISCUSSION

A. Short-range chemical order

Little or hardly any information is presently available about the effect of chemical short-range order on magnetic properties in Cr-rich Fe-Cr alloys, although many authors discussed the relevance of Fe clustering to magnetic measurements. Recently, Okano *et al.*[21] investigated the relationship between magnetoresistance and phase decomposition in Cr-Fe bulk alloys. The field-ion microscopy pictures clearly demonstrate how the tendency for Fe- clustering is reduced by progressive annealing followed by water quenching. In the present work, it is inferred that short-range chemical order influences the magnetic properties from the following findings.

(I) Variations of inverse low-field ac susceptibility with temperature are *not linear* even for temperatures well above T_C. The marked deviation from a Curie-Weiss behavior asserts that the description of $\chi^{-1}(T)$ in terms of non-interacting localized atomic moments is not possible. The existence of superparamagnetic clusters could account for the non-linearity.

(II) The application of a generalized[33] Curie-Weiss law yields an effective paramagnetic moment per alloy atom of $p_{\rm eff}=3.03\mu_B$ for heat-treated $Cr_{75}Fe_{25}$. Using the relation $p_{\rm eff}^2=q_c(q_c+2)$, the number of magnetic carriers per alloy atom[34] is $q_c=2.19$. In contrast, the saturation moment per alloy atom of $Cr_{75}Fe_{25}$ (at 5 K) is $q_s=0.41\mu_B$. The ratio $q_c/q_s>1$ combined with as low a value of Curie temperature as $T_C\sim 150$ K, is consistent with the Rhodes-Wohlfarth plot,[35] indicating that a simplified assumption of localized moments (Heisenberg model) does not hold. Instead, the alloys are *itinerant* ferromagnets. In the crossover concentration regime from ferromagnetism to a spin-glass state, a non-zero magnetic moment is only found[6,25] for Fe atoms. The magnetic moment per alloy atom at 4.2 K decreases with increasing Cr content. We find that, for the as-cast and heat-treated samples of $Cr_{75}Fe_{25}$ and $Cr_{70}Fe_{30}$, $\mu=0.41\mu_B$ and $0.54\mu_B$, respectively. These values agree quite well with those given previously by Aldred and Kouvel.[8] Therefore, chemical short-range order has only little, or even no, effect on the saturation moment per alloy atom at low temperatures. By contrast, at temperatures above T_C, chemical short-range order has a profound effect on low- as well as high-field properties (Fig. 6).

(III) Furthermore, there seems to be an intimate relation between the sharpness of the kink-point in low-field thermomagnetic data and chemical short-range order. This is inferred from the observation (Figs. 2 and 3) that the sharpening of the kink-point by annealing is a consequence of the decrease in the average Fe cluster size.

From (I), (II) and (III), it follows that short-range chemical order complicates the detection of the clearcut onset of long-range ferromagnetic order as finite magnetically or-

dered clusters persist for temperatures well above the FM-PM phase transition. The Curie temperature is defined as the temperature at which the spin-spin correlation length diverges, which, in turn, is crucial to the principle of scaling. Hence if the ratio of spins constituting the infinite cluster to those forming other magnetically ordered but finite clusters is low, as has been reported for several disordered crystalline magnetic alloys,[29] a greater sensitivity is required in a given measurement to detect the *onset* of long-range ferromagnetic order. As discussed in detail elsewhere,[29] an extrapolation to the zero field of the data taken at finite fields has to be taken with some caution, since the result depends on the field range chosen for extrapolation. Therefore, ''low-field'' or, better, ''zero-field'' methods are more appropriate for an analysis of critical magnetic properties. T_C and $\gamma_{\rm eff}$, determined by the low-field ac susceptibility data, are thus trusted the most. Zero-field small-angle neutron-scattering[10–12,16] data provide crucial information about the nature of phase transition if the temperature resolution is as good as in low-field ac susceptibility measurements, and if they probe correlations over an extended length scale such that an ''infinite'' cluster, if present, is detectable with ease.

On the other hand, the much-employed Mössbauer effect[1,2,9,13–16,18] probes the local environment. In metallurgically disordered systems such as Cr-Fe alloys that show chemical clustering, special care[36] has to be taken to interpret the observations. A ''slow transition,'' described by a broad temperature interval between PM and FM states, might appear due to the different local environments in chemically inhomogeneous systems. Such data cannot completely rule out[17–19] the possible existence of an infinite ferromagnetic cluster. Here again, one has to consider the problem of sensitivity in identifying the *onset* the infinite ferromagnetic cluster within an environment of magnetic disorder.

B. Long-range ferromagnetic order

The spatial variation in chemical composition was smeared out by annealing the sample and subsequently quenching it in water. While microprobe analysis is limited in spatial resolution as well as in chemical composition determination, and hence in recognizing homogenizing effects, magnetic methods are *sensitive* to (average) changes in chemical clustering (in the present case, Fe); the chemical local environment determines (local) magnetic ordering and hence the effective macroscopic magnetic properties of the alloy under consideration. The temperature dependence of low-field magnetic measurements is a powerful tool in probing changes in chemical short-range order. Chemical and magnetic analyses show that the chosen heat treatments successfully homogenize the chemical composition of the samples. Low-field ac susceptibility measurements demonstrate that the kink-point temperature T_k reduces, and that the kink point sharpens after heat treatment followed by a water quench. In accordance with the outcome of microprobe analysis, this indicates that Fe clusters are reduced in number and Cr dissolves more homogeneously in the alloy matrix.

For the $Cr_{75}Fe_{25}$ sample, the temperature dependence of low-field susceptibility coincides up to 10% of T_k with that reported in Ref. 12, (Fig. 20). For $Cr_{70}Fe_{30}$, the sharpness of the kink point is even increased. Hence, the quality of our annealed samples in terms of chemical homogeneity, as measured by the sharpness of the low-field susceptibility kink point, compares well with that of other groups.[7,12] The following observations support the view that long-range ferromagnetic order exists in the alloys under consideration.

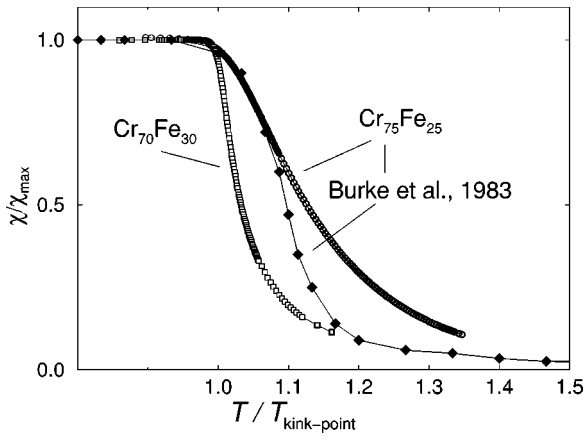

FIG. 20. Low-field susceptibility kink point of the best-possible chemically homogenized specimen. Similar data on a chemically homogenized $Cr_{75}Fe_{25}$ polycrystal, from Burke and Rainford (Ref. 12), are also shown for comparison.

(I) A demagnetization-limited low-field susceptibility χ and a well-defined decrease of $\chi(T)$ (the kink point) indicate that the alloys prepared satisfy the first requirement of the critical-point analysis. The demagnetizing factors determined in present experiments are close to that of an ideally homogeneously magnetized sphere. Thus the arguments given by Beck[17] are not relevant, since the different degrees of sharpness in kink-point measurements in perpendicular and in-plane geometry of a disk can be accounted for[28] easily.

(II) To distinguish between a freezing of superparamagnetic clusters, as proposed by Beck,[17] and a true FM-PM phase transition, the frequency dependence of the initial ac susceptibility was studied. No shift in kink-point temperature could be detected for frequencies ν, varying from 7 to 1000 Hz, of the ac driving field of rms amplitude 0.1 mT. For the superparamagnetic clusters description, a quantitative measure[37] of the frequency shift in the ''freezing'' temperature T_f is given by $(\Delta T/T_f)$ per decade of ν. As the present measurements (Fig. 4) allow a distinction of shift in temperature better than 0.1% of T_k, freezing of superparamagnetic clusters as the origin for the kink seems to be an unlikely explanation. Instead, a cooperative ordering at T_k, of spins yielding an infinite long-range ferromagnetic cluster, is strongly indicated by these experiments. The unresolved deviations between T_1 and T_2 [both well above $T_k(\sim T_C)$] are attributed to different response signals generated by the fluctuating superparamagnetic clusters which come into existence when an infinite cluster breaks up into smaller clusters at such temperatures. This interpretation also accounts for the non-Curie-Weiss behavior at even $\sim 2\ T_C$. In view of the above arguments, long-range ferromagnetic order is anticipated for temperatures below T_C.

TABLE II. Comparison between experiment and theory.

Critical exponent	Experiment			Theory						
				$J(r)\sim e^{-r/b}$ References 39 and 40				$J(r)\sim r^{-(d+\sigma)}$ Reference 42		
	$Cr_{75}Fe_{25}$	$Cr_{70}Fe_{30}$	Fe Ref. 38	$d=3$ $n=1$	$d=3$ $n=2$	$d=3$ $n=3$	$d=2$ $n=1$	$\sigma=1.4$ $d=2$ $n=1$	$\sigma=1.325$ $d=2$ $n=2$	$\sigma=1.285$ $d=2$ $n=3$
α	-	-	-	0.110(5)	−0.007(6)	−0.115(9)	0.00	0.012	−0.097	−0.162
β	0.30(1)	0.315(5)	0.389(5)	0.325(2)	0.346(2)	0.365(3)	0.125	0.298	0.354	0.386
γ	1.39(1)	1.39(1)	1.333(1)	1.241(2)	1.316(3)	1.386(4)	1.75	1.392	1.389	1.389
δ	5.5(1)	5.36(4)	4.35(5)	4.82(3)	4.81(3)	4.80(4)	15.0	5.67	4.93	4.59

C. Ferromagnetic-paramagnetic phase transition

From the outcome of the methods of analyses of the bulk magnetization and low-field ac susceptiblity data, we conclude that the homogenized heat-treated $Cr_{75}Fe_{25}$ and $Cr_{70}Fe_{30}$ alloys are systems that exhibit long-range ferromagnetic order, and undergo a thermodynamic phase transition from a ferromagnetic state to a paramagnetic state at a well-defined transition temperature T_C. The present bulk magnetization measurements carried out on well-homogenized alloys allow an accurate determination of the effective critical exponents that fulfill the scaling relations, indicating a true phase transition in homogenized $Cr_{75}Fe_{25}$ and $Cr_{70}Fe_{30}$ alloys. The transition is characterized by *effective* critical exponents $\beta_{\rm eff}=0.30(1)$, $\gamma_{\rm eff}=1.39(1)$, and $\delta_{\rm eff}=5.4(1)$. These are not significantly different from the true *asymptotic* critical exponents, as T_C has been approached as closely as 6×10^{-4} in reduced temperature ϵ in most of the experimental runs. In Table II, these values are compared with those previously determined[38] for crystalline Fe in roughly the same reduced temperature range as the present one, and with the best theoretical estimates[39,40] for $d=3$ ferromagnets with $n=1$, 2, and 3, in which spins are coupled by the ''short-range'' exchange interactions of the Heisenberg type, $J(r)\sim e^{-r/b}$. Such a comparison reveals that the presently determined exponent values, though close to those theoretically predicted for a three-dimensional isotropic short-range (ISR) Heisenberg ferromagnet (i.e., for $d=n=3$ system), are shifted *away* from the mean-field (MF) estimates of $\beta=0.5$, $\gamma=1.0$, and $\delta=3.0$. By contrast, the exponent values reported[38] for Fe (Table II), *like* those[41] [$\beta=0.395(10)$, $\gamma=1.345(10)$, $\delta=4.35(6)$] for Ni, are shifted *toward* the MF magnitudes. Such a shift observed in the itinerant-electron ferromagnets Fe and Ni is a manifestation[41] of the *isotropic long-range* (ILR) exchange interactions of the form $-(J_\infty/r^{d+\sigma})\,\mathbf{S_0}\cdot\mathbf{S_r}$ (where $0<\sigma<2$) which render the ISR $d=3$ Heisenberg fixed point unstable and lead to a *crossover*[42] to the ILR fixed point, which is characterized by exponent values that are *ISR* $d=3$ Heisenberg-like but shifted *toward* the MF values. The deviations from the MF exponent values observed in the present case may as well indicate the presence of isotropic long-range exchange interactions in the itinerant-electron ferromagnets under consideration.

Effective exponent values similar to the presently determined ones were previously reported[43–46] for amorphous Cr or Mn-based Fe-containing alloys with composition near the percolation threshold for long-range ferromagnetic order. Apart from similar magnitudes of the effective exponents, the property that these crystalline and amorphous Cr-Fe alloys have in common is that only a *small fraction* of the total number of magnetic moments actually participates in the ferromagnetic-paramagnetic phase transition (Table I).

This phenomenon, prevalent in a host[29] of the other disordered spin systems that exhibit reentrant behavior at low temperatures, finds a straightforward explanation in terms of the *infinite* FM network (matrix) plus *finite* FM spin clusters model,[29,36] as detailed elsewhere.[29,47] With barely 1% of total spins constituting the infinite FM network in the presently investigated CrFe alloys (Table I) [in crystalline Fe or Ni (Ref. 41)], the network is expected to be *highly ramified*. As a consequence, the infinite FM network has an effective topological dimensionality of $d<3$, the probability for the existence of nearest-neighbor (NN) moment pairs is small and the average intermoment spacing is far greater than the NN distance ($r_{\rm NN}$).

In a spin system with an effective space dimensionality of $d<3$, e.g., $d=2$, and intermoment spacing $>r_{\rm NN}$, short-range (Heisenberg) exchange interactions cannot[40] support long-range ferromagnetic order. The only exception to this rule is the two-dimensional ($d=2$) Ising ($n=1$) case for which the critical exponents possess values (Table II), that are quite different from those determined in this work. At distances far greater than $r_{\rm NN}$, only *long-range* interactions can provide an effective means of coupling the spins in the infinite network, and thereby sustain long-range ferromagnetic order in the alloys in question. This consideration lead us to explore the possibility of applying the model,[42] in which the *isotropic* long-range exchange interactions of the form $-(J_\infty/r^{d+\sigma})\,\mathbf{S_0}\cdot\mathbf{S_r}$ (where $0\leqslant\sigma\leqslant2$) couple spins, to the present case. The critical exponent values for two-dimensional ($d=2$) ferromagnets with $n=1$, 2, and 3, displayed in Table II, are arrived at as follows. The parameter σ is chosen such that the expression for the exponent γ given in Ref. 42 yields a value ($\simeq1.39$) close to that observed experimentally and the remaining exponents are calculated by inserting the value of σ, so obtained, in the expressions

$\eta=2-\sigma$ and $\nu=\gamma/\sigma$ and by using the scaling equalities $\alpha=2-\nu d$, $\beta=(2-\alpha-\gamma)/2$ and $\delta=1+(\gamma/\beta)$. Even a cursory glance at the entries in Table II suffices to reveal that the presently determined exponent values match those theoretically predicted[42] for a $d=2$, $n=1$ ferromagnet in which the attractive interaction between the spins decays with distance (r) as $J(r)\sim r^{-3.4}$. Strong experimental evidence for the premise that the asymptotic critical behavior of the itinerant ferromagnets in question corresponds to a spin system with space dimensionality of $d=2$ is provided by our observation that $Cr_{70}Fe_{30}$ thin film of thickness 94 Å (a quasi-*two-dimensional* system) exhibits the *same* critical behavior[48] as its bulk counterpart.

Next we discuss the possible origin of the discrepancy between the values of $\beta_{\rm eff}$ and $\gamma_{\rm eff}$ determined in this work and those previously reported. Granting that in both cases equally well-homogenized samples were used, the method of analyzing magnetic isotherms employed by Aldred and Kouvel[8] suffers from two main drawbacks. First, the nonlinear extrapolation method used to obtain the ''zero-field'' quantities J_S and χ_0 gives rise to large systematic errors,[29] particularly in $J_S(T)$. Second, magnetic isotherms were taken[8] at 1-K temperature intervals. It is well known that the asymptotic critical regime normally spans temperatures within 1% and 2% of T_C, and hence the extracted exponent values in Ref. 8, far from being asymptotic exponents, are at best effective exponent values obtained in a temperature range outside the asymptotic critical regime. It is evident from Fig. 5 that an unusually large value $\gamma\simeq 2$ (similar to that reported[8] earlier) outside the asymptotic critical region is possible for chemically disordered alloys.

Burke and co-workers[11,12] have discussed magnetic properties of these alloys within the framework of percolation theory. Neutron-scattering experiments[11,12] yielded a value as large as $\nu=1.2$ for the correlation length critical exponent. By assuming the exponent η, which describes the variation of the spin-spin correlation function with distance at T_C, to be zero ($\eta=0$) and making use of the scaling relation $\gamma=\nu(2-\eta)$, Burke and co-workers[11,12] concluded that their value of ν is consistent with the anomalously large value of $\gamma\simeq 2$ obtained earlier by Aldred and Kouvel.[8] The present values $\gamma=1.39\pm0.01$ and $\eta=2-\sigma=2-1.4=0.6$ when used in the above scaling relation, yield a value $\nu=0.99\pm0.01$, which is close to that ($\nu=1.2\pm0.1$) determined previously from the neutron scattering experiments.[11,12]

V. SUMMARY

This work presents a detailed reappraisal of the magnetic critical behavior of polycrystalline $Cr_{75}Fe_{25}$ and $Cr_{70}Fe_{30}$ based on an elaborate analyses of high-precision bulk magnetization and, for the first time to our knowledge, low-field ac susceptibility data. Annealing followed by quenching in water diminishes the chemical clustering to a large extent. Homogenized, but highly disordered, $Cr_{75}Fe_{25}$ and $Cr_{70}Fe_{30}$ alloys show long-range ferromagnetic order below a well-defined Curie-temperature.

The FM-PM transition is characterized by critical exponents that deviate substantially from those predicted by $d=3$ or 2 isotropic ''short-range'' models, but coincide in magnitude with the ones yielded by the renormalization group calculations[42] for a $d=2$, $n=1$ spin system with long-range attractive interactions between spins decaying as $J(r)\sim r^{-(d+\sigma)}$ with $\sigma=1.4$. This finding is consistent with the itinerant character of ferromagnetism in $Cr_{75}Fe_{25}$ and $Cr_{70}Fe_{30}$ alloys, as inferred from a large q_C/q_S ratio.

ACKNOWLEDGMENTS

The authors are thankful to P. Keppler, R. Henes, and W. Maisch for ingot and sample preparation, and B. Meyer, C. Hofer, S. Haug, and S. Kühnemann for chemical analysis and microanalysis. S.F.F. is indebted to W. Donner for discussions concerning neutron-diffraction experiments. S.N.K. gratefully acknowledges the financial support of the Max-Planck-Society, and the hospitality of the Max-Planck-Institut für Metallforschung, Stuttgart.

*Present address: Werkstoffe der Elektrotechnik, Ruhr-Universität Bochum, 44780 Bochum, Germany.

[1] J. Hesse and U. Schossow, Int. J. Magn. **5**, 187 (1973).
[2] J. Hesse and A. Rübartsch, Physica B & C **80**, 33 (1975).
[3] B. Loegel, J. Phys. F: Met. Phys. **5**, 497 (1975).
[4] B. Loegel, J. M. Friedt, and R. Poinsot, J. Phys. F: Met. Phys. **5**, L54 (1975).
[5] A. T. Aldred, Phys. Rev. B **14**, 219 (1976).
[6] A. T. Aldred, B. D. Rainford, J. S. Kouvel, and T. J. Hicks, Phys. Rev. B **14**, 228 (1976).
[7] R. D. Shull and P. A. Beck, in *Magnetism and Magnetic Materials*, edited by C. D. Graham, G. H. Lander, and J. J. Rhyne, AIP Conf. Proc. No. 24 (AIP, New York, 1975), p. 95.
[8] A. T. Aldred and J. S. Kouvel, Physica B & C **86-88**, 329 (1977).
[9] M. Shiga and Y. Nakamura, J. Phys. Soc. Jpn. **49**, 528 (1980).
[10] S. K. Burke and B. D. Rainford, J. Phys. **13**, 441 (1983).
[11] S. K. Burke, R. Cywinski, J. R. Davies, and B. D. Rainford, J. Phys. **13**, 451 (1983), and references cited therein.
[12] S. K. Burke and B. D. Rainford, J. Phys. **13**, 471 (1983).
[13] S. M. Dubiel, Ch. Sauer, and W. Zinn, Phys. Rev. B **30**, 6285 (1984).
[14] S. M. Dubiel, Ch. Sauer, and W. Zinn, Phys. Rev. B **31**, 1643 (1985).
[15] S. M. Dubiel, K. H. Fischer, Ch. Sauer, and W. Zinn, Phys. Rev. B **36**, 360 (1987).
[16] D. Boumaouza, Ph. Mangin, B. George, P. Louis, R. A. Brand, J. J. Rhyne, and R. W. Erwin, Phys. Rev. B **39**, 749 (1989).
[17] P. A. Beck, Phys. Rev. B **39**, 752 (1989).
[18] C. Bansal, T. Kumaran, S. J. Campbell, and G. L. Whittle, Phys. Rev. B **44**, 7111 (1991).
[19] P. A. Beck, Phys. Rev. B **44**, 7115 (1991).
[20] R. A. Brand, Phys. Rev. B **44**, 7117 (1991).
[21] R. Okano, K. Hono, K. Takanashi, H. Fujimori, and T. Sakurai, J. Appl. Phys. **77**, 5843 (1995).
[22] G. Frollani, F. Menzinger, and F. Sacchetti, Phys. Rev. B **11**, 2030 (1975).
[23] H. Hasegawa, J. Phys. Soc. Jpn. **50**, 802 (1981).
[24] T. Jo, J. Magn. Magn. Mater. **31-34**, 51 (1983).

[25] Y. Kakehashi, Phys. Rev. B **35**, 4973 (1987).
[26] M. E. Elzain, J. Phys.: Condens. Matter **3**, 2089 (1994).
[27] V. N. Gittsovich, V. G. Semenov, and V. M. Uzdin, J. Magn. Magn. Mater. **146**, 165 (1995).
[28] P. J. Wojtowicz and M. Rayl, Phys. Rev. Lett. **20**, 1489 (1968).
[29] S. N. Kaul, J. Magn. Magn. Mater. **53**, 5 (1985); IEEE Trans. Magn. **20**, 1290 (1984).
[30] A. Arrott, Phys. Rev. **108**, 1394 (1957).
[31] A. Arrott and J. E. Noakes, Phys. Rev. Lett. **19**, 786 (1967).
[32] J. S. Kouvel and M. E. Fisher, Phys. Rev. **136**, A1626 (1964).
[33] S. N. Kaul, Phase Transit. **47**, 23 (1994); M. Sambasiva Rao and S. N. Kaul, J. Magn. Magn. Mater. **171**, 341 (1997).
[34] E. P. Wohlfarth, J. Magn. Magn. Mater. **7**, 113 (1978).
[35] P. Rhodes and E. P. Wohlfarth, Proc. R. Soc. London, Ser. A **273**, 247 (1963).
[36] S. N. Kaul, Solid State Commun. **36**, 279 (1980); Phys. Rev. B **22**, 278 (1980).
[37] J. A. Mydosh, *Spin Glasses: An Experimental Introduction* (Taylor & Francis, London, 1993), p. 64ff.
[38] A. Arajs, B. L. Tehan, E. E. Anderson, and A. A. Stelmach, Int. J. Magn. **1**, 41 (1970).
[39] J. C. LeGuillou and J. Zinn-Justin, Phys. Rev. B **21**, 3976 (1980).
[40] M. E. Fisher, Rev. Mod. Phys. **46**, 597 (1974).
[41] M. Seeger, S. N. Kaul, H. Kronmüller, and R. Reisser, Phys. Rev. B **51**, 12585 (1995).
[42] M. E. Fisher, S. K. Ma, and B. G. Nickel, Phys. Rev. Lett. **29**, 917 (1972).
[43] M. Olivier, J. O. Strom-Olsen, Z. Altounian, and G. Williams, J. Appl. Phys. **53**, 7696 (1982).
[44] P. Hargraves and R. A. Dunlap, J. Magn. Magn. Mater. **75**, 378 (1988).
[45] U. Güntzel and K. Westerholt, Phys. Rev. B **41**, 740 (1990).
[46] J. A. Geohegan and S. M. Bhagat, J. Magn. Magn. Mater. **25**, 71 (1980); M. A. Manheimer, S. M. Bhagat, and H. S. Chen, J. Magn. Magn. Mater. **38**, 147 (1983).
[47] S. N. Kaul, J. Phys.: Condens. Matter **3**, 4027 (1991); P. D. Babu and S. N. Kaul, *ibid.* **9**, 7189 (1997); S. N. Kaul and P. D. Babu, *ibid.* **10**, 1563 (1998).
[48] S. F. Fischer, S. N. Kaul, and H. Kronmüller, J. Magn. Magn. Mater. **226-230**, 540 (2001).